sustainability

MDPI

Article

Influence of the Steel Slag Particle Size on the Mechanical Properties and Microstructure of Concrete

Maohui Li [1,*], Youjun Lu [1,*], Yajuan Liu [2], Jingjun Chu [2], Tongsheng Zhang [3] and Wei Wang [4]

[1] School of Materials Science and Engineering, North Minzu University, Yinchuan 750021, China
[2] Ningxia Saima Kejin Concrete Co., Ltd., Yinchuan 750001, China; lyj130129@163.com (Y.L.); cjingjun123456@163.com (J.C.)
[3] School of Materials Science and Engineering, South China University of Technology, Guangzhou 510641, China; mstszhang@scut.edu.cn
[4] Ningxia Hui Autonomous Region Construction Engineering Quality and Safety General Station, Yinchuan 750004, China; nxwwt2005@126.com
* Correspondence: lmnlmb@nmu.edu.cn (M.L.); youjunlu518@hotmail.co (Y.L.)

Abstract: The present paper probes into the influence of the steel slag particle size on the mechanical properties and microstructure of concrete, with steel slag serving as the primary raw material. Steel slag with different particle sizes was selected as the partial substitute material for concrete by mechanical grinding. The influence of steel slag on the compressive strength, bending strength, and microstructure of concrete was determined by laser particle size analyzer, specific surface area analyzer, strength experiment, X-ray diffraction (XRD), and scanning electron microscope (SEM). The results show that mechanical grinding has significant effects on the particle size distribution and specific surface area of the steel slag. The optimal grinding time is 20 min and the specific surface area is 0.65 m^2/g. D10, D50 and D90 are 0.91 μm, 16.57 μm and 46.40 μm, respectively. The steel slag with a fine particle size can better fill the pores in concrete and improve the compactness, thus enhancing the mechanical properties of concrete. The change in the steel slag particle size does not change the type of hydration products, but the smaller the particle size of steel slag, the better the gelling activity, the larger the hydration products, the denser the structure, and the better the mechanical properties. Therefore, the present study provides an important theoretical basis and practical guidance for the application of steel slag as an additive in the concrete industry.

Keywords: steel slag particle size; concrete; mechanical properties; microstructure; admixture

check for updates

Citation: Li, M.; Lu, Y.; Liu, Y.; Chu, J.; Zhang, T.; Wang, W. Influence of the Steel Slag Particle Size on the Mechanical Properties and Microstructure of Concrete. *Sustainability* **2024**, *16*, 2083. https://doi.org/10.3390/su16052083

Academic Editor: Constantin Chalioris

Received: 16 December 2023
Revised: 19 February 2024
Accepted: 23 February 2024
Published: 2 March 2024

Copyright: © 2024 by the authors. Licensee MDPI, Basel, Switzerland. This article is an open access article distributed under the terms and conditions of the Creative Commons Attribution (CC BY) license (https://creativecommons.org/licenses/by/4.0/).

1. Introduction

In the field of construction materials science, optimization of concrete properties has always been an important issue [1,2]. With the increasing emphasis on environmental sustainability, the utilization of industrial by-products to improve concrete properties is not only a way to enhance resource recycling but also an important direction for the innovation of traditional construction materials [3–5].

Steel slag is the solid waste produced by smelting steel, which is the product of slag-making agents added for deoxidation, desulfurization, and dephosphorization in steelmaking, and the emissions account for about 12% to 20% of steel production. At present, the utilization rate of steel slag in China is less than 30%, and there is a big gap with the utilization rate of nearly 100% in developed countries such as the United States and Germany. The comprehensive utilization of steel slag resources can not only reduce the pollution to the environment but also produce benefits for iron and steel enterprises. The main chemical components of steel slag are CaO, SiO_2, Fe_2O_3, MgO, and Al_2O_3, of which the active components are CaO, SiO_2, and Al_2O_3, and the higher the content, the better the activity of steel slag [6,7]. Researchers have explored the use of steel slag in concrete, focusing on the effect of steel slag admixture on concrete properties such as

density, strength, and durability [8–10]. Nan et al. [11] explored the mechanical properties, hydration products, and the process of hydration hardening of concrete prepared by combining steel slag with mineral slag. The study found that the concrete exhibited optimal mechanical properties when the steel slag content was 31.97%, with 28-day compressive and flexural strengths of 20.20 MPa and 7.25 MPa, respectively. Liu et al. [12] successfully developed alkali-activated slag/steel slag cementitious materials using silica fume and alkali slag. The optimal mix achieved 28-day compressive and flexural strengths of 36.2 MPa and 13.29 MPa, respectively, satisfying the requirements for ordinary slag Portland cement of grade 32.5. Masilamani et al. [13] carried out a study on the difference in performance between EOF steel slag and natural aggregate, and they compared the difference in the shape index, roundness, sphericity, form factor, and roundness of the two materials. The results showed that different grading size ranges of EOF steel slag, a hardened interface zone, and a rough surface texture were beneficial to the improvement of concrete strength.

Lai et al. [14] used BOF steel slag to replace coarse aggregate and fine aggregate, and their results showed that the optimal replacement rates of coarse aggregate and fine aggregate were 50% and 30%, respectively. Under these replacement rates, the late compressive strength and microstructure of concrete were significantly improved.

Current research shows that steel slag can enhance its cementitious activity through chemical and mechanical activation, and it performs well when incorporated into products like concrete [15–19]. However, most studies have focused on the overall amount of steel slag added, and relatively few studies have been carried out on the effect of the key factor of the steel slag particle size [20,21]. The properties of steel slag, such as the particle size, distribution curve, and specific surface area, determine the gelling activity of steel slag. Variations in the particle size of steel slag can significantly affect the microstructure of concrete, subsequently impacting its macroscopic mechanical properties. It is significant to study the influence of the change in the steel slag particle size on the mechanical properties and microstructure of concrete. Therefore, the present study is dedicated to investigating the influence law of the steel slag particle size on the mechanical properties and microstructure of concrete.

The present paper involves grinding steel slag for varying durations to achieve different particle sizes, and then mixing it with cement and standard sand to prepare concrete. Through a comprehensive analysis of experimental data, this study investigates the effects of the steel slag particle size on crucial mechanical characteristics such as the compressive strength, flexural strength, and the microstructure of concrete. Accordingly, this research aims to provide new theoretical insights and practical guidelines for optimizing concrete properties and to offer novel perspectives on the effective use of industrial by-products in building material applications.

2. Materials and Methods

2.1. Experimental Materials

The steel slag utilized in this study was an industrial solid waste obtained from the basic oxygen furnace (BOF) slag of a steel corporation in Ningxia. A comprehensive chemical composition analysis of the steel slag was performed, the results of which are detailed in Table 1. Figure 1 illustrates the morphology and phase composition of the steel slag, characterized by an approximate size of 1 cm, heterogeneous coloration, and predominantly irregular, angular morphologies. The primary phases identified in the steel slag were C_3S (Tricalcium Silicate) and C_2S (Dicalcium Silicate), along with minor constituents of the RO phase and Fe_3O_4 (magnetite). The cement selected for the experimental purposes was Saima brand (Grade 425 R) produced by Ningxia Saima Cement Co., Ltd. (Yinchuan, China), and the sand employed was standard sand manufactured by Xiamen Aisou Standard Sand Co., Ltd. (Xiamen, China).

Table 1. Chemical composition of the steel slag.

Oxides	CaO	Fe_2O_3	MnO	SiO_2	MgO	Al_2O_3	P_2O_5	Others
Wt %	36.79	16.38	6.36	18.97	9.20	4.19	0.07	6.03

Note: Others, including TiO_2, Na_2O, K_2O, and ignition loss, were not analyzed.

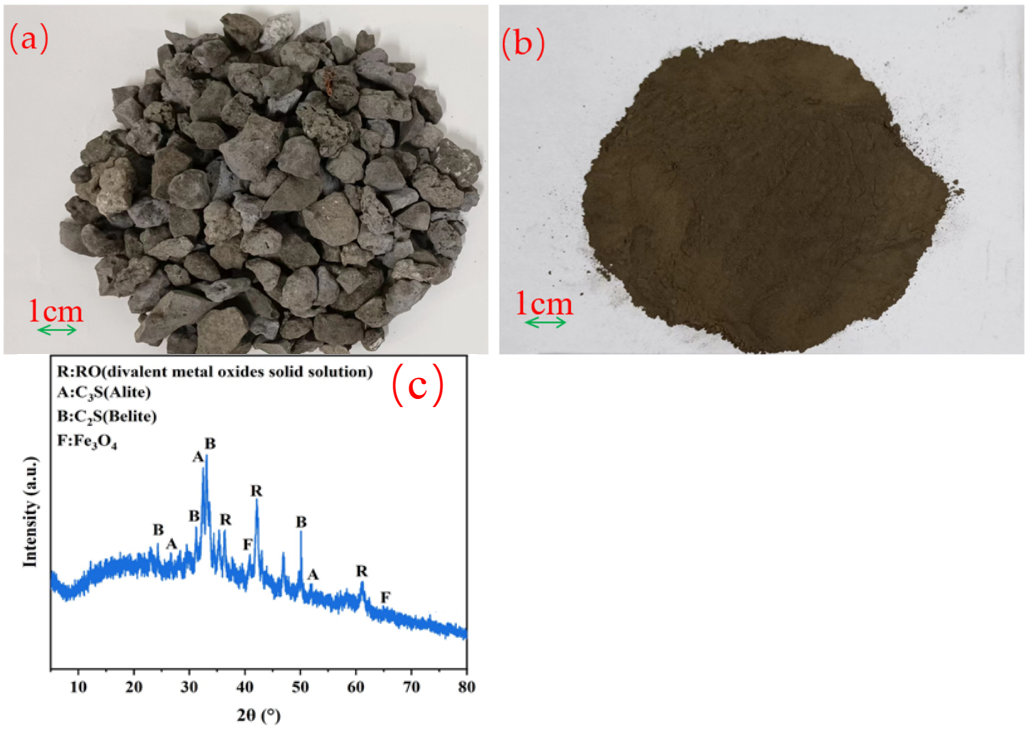


Figure 1. Morphology of the steel slag and XRD spectrum: (**a**) raw steel slag, (**b**) grind steel slag for 10 min, and (**c**) XRD spectrum of steel slag.

In accordance with the findings deduced from the Equation as referenced in [22], the steel slag's alkalinity coefficient was quantitatively assessed as 2.22. This numerical value, which surpasses the threshold of 1.8 yet remains beneath the upper limit of 2.5, categorically places this specific steel slag within the ambit of medium basicity slags. (See Table 2).

Table 2. Classification of the steel slag by basicity.

Steel Slag	Alkalinity Coefficient
High basicity slag	$R < 1.8$
Medium basicity slag	$1.8 < R < 2.5$
Low basicity slag	$R > 2.5$

2.2. Sample Preparation

The steel slag obtained from the enterprise was ground using a hermetic sample mill (HFZY-F4). The grinding durations were 10 min, 20 min, 30 min, 40 min, and 50 min. The ground steel slag was then sieved through a 200-mesh screen to obtain the required steel slag powder. The particle size, phase composition, specific surface area, and micro-morphology of the steel slag powder were then tested. The ground steel slag was mixed with Portland cement to prepare concrete. The experimental plan is given in Table 3.

Table 3. Mix proportioning scheme for the steel slag concrete.

No.	Grinding Time/min	Cement/g	Steel Slag/g	Standard Sand/g	Water/Cement Ratio
S0	--	450	0	1350	0.4
S1	10	360	90	1350	0.4
S2	20	360	90	1350	0.4
S3	30	360	90	1350	0.4
S4	40	360	90	1350	0.4
S5	50	360	90	1350	0.4

(1) Weigh steel slag, cement, standard sand, and water according to Table 3, pour into the cement sand mixing experimental equipment, and turn slowly, transfer, and fast for the 60 s in turn to complete the concrete mixing work.

(2) Load the mix into the mold (400 mm × 400 mm × 1600 mm), pound the mix around the mold with a spatula, put the test mold on the shaking table, and level the vibration for 60 s, to avoid beating during the vibration process, when the cement slurry stops, to prevent segregation caused by over-vibration.

(3) Put the test mold into the standard constant temperature and humidity curing box for 24 h and remove the mold for standard maintenance. The curing condition is 20 ± 2 °C and the humidity is 95%. The space between 10 and 20 mm should be maintained on the support for the test specimen.

2.3. Test Methods

The particle size distribution of the ground steel slag was measured using a laser particle size analyzer (Bettersize 2000, Dandong Co., Dandong, China). In parallel, the specific surface area of the steel slag powder was determined using a specific surface area analyzer (3H-2000 A, Beishide Co., Beijing, China). The crystal structure of the raw materials and ceramic samples was detected at a scanning rate of 4°/min and an angle range of 10~80° by a model XRD-6000 X-ray diffractometer (XRD, Shimadzu Co., Kyoto, Japan). The intricate microstructural characteristics of these samples were closely examined and captured utilizing an advanced thermal field emission scanning electron microscope (SEM, Zeiss Co., Jena, Germany). In addition, the flexural strength and compressive strength of the samples were tested using a universal testing machine (YAW-300 C, Jianli Co., Zhuji, China). The quantification of the compressive strength was conducted in accordance with the maximum force by the cross-sectional area, whereas the flexural strength was calculated by adhering strictly to the guidelines set forth in Formula (1).

$$P = \frac{FL}{bh^2} \quad (1)$$

where P—represents the flexural strength (MPa), F—specimen failure load (N), L—indicates the span between supports (mm), h—represents the section height of the specimen (mm), and b—section width of the specimen (mm).

3. Results and Discussion

3.1. Effect of Grinding Time on Steel Slag Particle Size

The changes in the specific surface area, particle size distribution, and morphology of steel slag after grinding for different durations are shown in Table 4 and Figures 2 and 3. D10, D50, and D90 represent the meaning of 10%, 50%, and 90% of the particle size in the measured size value. Specifically, Figure 2a presents the particle size distribution of steel slag after different grinding times, while Figure 2b illustrates the cumulative trend of the particle sizes for steel slag ground for varying durations.

Table 4. Specific surface area and particle size of the steel slag at different grinding times.

No.	Specific Surface Area/(m^2/g)	Particle Size/μm		
		D10	D50	D90
S1	0.64	2.05	21.31	126.40
S2	0.65	0.91	16.57	46.40
S3	0.56	1.03	21.85	127.60
S4	0.51	1.06	24.57	152.60
S5	0.45	1.42	31.55	172.20

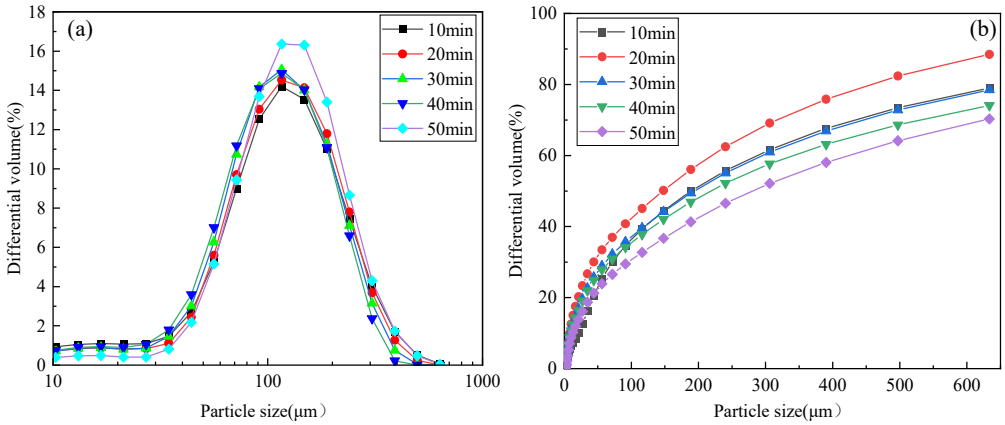


Figure 2. Steel slag particle size distribution trends at different grinding times: (**a**) particle size distribution; and (**b**) the cumulative trend of particle sizes.

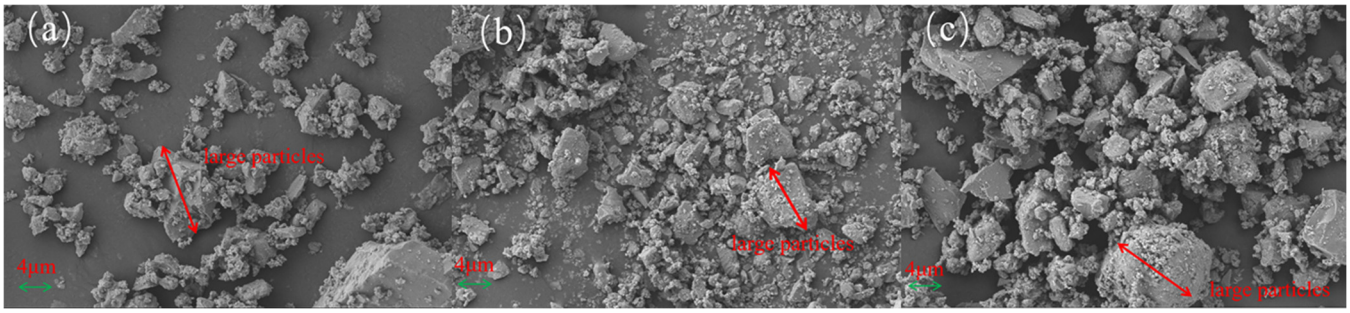


Figure 3. Changes in the steel slag morphology under different grinding times: (**a**) grinding 10 min; (**b**) grinding 20 min; and (**c**) grinding 50 min.

According to Table 3 and Figure 2, it can be seen that due to the intense collision and grinding action of mechanical milling, the particles of the steel slag interact with each other. As the grinding time increases, the specific surface area first increases and then decreases, while the particle size decreases first and then increases. The distribution of the steel slag particles becomes narrower and more concentrated, and the cumulative curve of the particle size gradually shifts to the left [23]. When the grinding time reaches 20 min, the specific surface area peaks at 0.65 m^2/g; D10, D50, and D90 are 0.91 μm, 16.57 μm, and 46.40 μm, respectively. Upon surpassing the 20 min threshold in the grinding duration, a majority of the steel slag particles undergo a significant diminution, being meticulously pulverized into finer granules. Persisting in extending the grinding interval subsequently instigates a propensity for the surfaces of these microscopically diminutive particles to adhere to one another, catalyzing a pronounced agglomerative phenomenon. This leads to a discernible contraction in the specific surface area, alongside a gradual augmentation in the particle size. Such observations are indicative of the grinding process transitioning into a state of dynamic equilibrium, characterized by the complex interplay of fragmentation,

refinement, agglomeration, and coarsening, wherein the latter two processes progressively dominate the particle size dynamics [24].

Figure 3 eloquently illustrates that as the duration of mechanical grinding extends, a significant portion of the larger particles within the steel slag powder are subjected to a substantial reduction in size, leading to an increased prevalence of finer granules. Notably, even amidst the extensive grinding process, the persistence of distinctly visible larger particles is observed. This phenomenon in the mechanical grinding of steel slag can be attributed to the inherent variability in the grindability amongst its different phases. Specifically, phases characterized by poor grindability exhibit a marked resistance to pulverization, thus remaining relatively intact, whereas those phases with enhanced grindability are more readily and efficiently reduced into smaller particles [25].

After 10 min of grinding (Figure 3a), compared to the original steel slag particles, the size of the steel slag particles begins to decrease and their morphology presents an irregular polygonal block shape, with still visibly large particles. When the grinding time increases to 20 min (Figure 3b), the irregular large particles are further refined, the number of small particles significantly increases, the particle size becomes more uniform, the edges and corners of the particles shrink, and their appearance becomes rounder. With an increase in grinding time to 50 min (Figure 3c), the steel slag particles do not become smaller but instead slightly increase in size, tending toward a more spherical shape. Combining this with the particle distribution curve in Figure 2, it can be inferred that with a further increase in grinding time, the steel slag particles undergo agglomeration. The simultaneous occurrence of particle refinement and agglomeration leads to an increase in the average particle size.

3.2. Influence of the Particle Size on the Mechanical Properties

The variation in the compressive strength and flexural strength of steel slag concrete at curing ages of 3 days, 7 days, and 28 days is shown in Figure 4. Specifically, graph (a) illustrates the compressive strength, while graph (b) depicts the flexural strength.

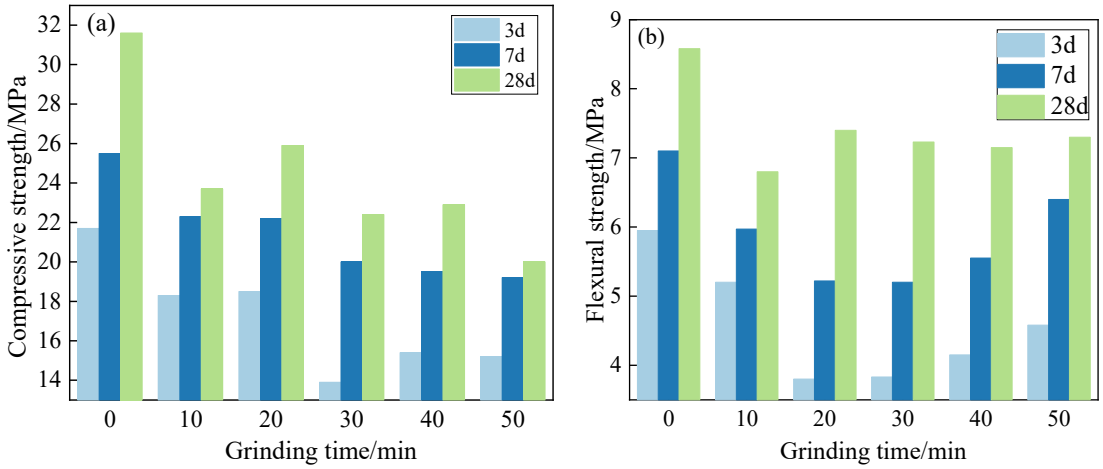


Figure 4. Compressive strength and flexural strength of the steel slag concrete: (**a**) the compressive strength; and (**b**) the flexural strength.

In Figure 4, compared to the control group without steel slag addition (the group where the grinding time is 0 min), both the compressive strength and flexural strength of the concrete with steel slag inclusion show a decrease. As the grinding time increases, the compressive strength of the steel slag concrete initially increases and then decreases, while the flexural strength generally shows a trend of initial increase followed by stabilization. When the grinding time increases from 10 min to 20 min, both the 28-day compressive strength and flexural strength of the steel slag concrete increase, reaching 25.95 MPa and 7.40 MPa, respectively. These results are higher than the compressive and flexural strengths

of the same steel slag admixture (No. 20SL) in reference [26]. One of the reasons is that the water/cement ratio in this paper (0.4) is lower than that in the reference (0.58), and the other reason is that the steel slag particles in this paper have a finer particle size and larger specific surface area. The changes in the 7-day and 3-day flexural and compressive strengths are not significant and even show a downward trend. This is because the steel slag material itself has relatively low reactivity. Although mechanical grinding reduces the particle size and slightly increases the activity, the initial reactivity remains low, resulting in a weaker rate of hydration reaction. However, as the curing age increases, the reactivity of the steel slag gradually manifests, leading to an improvement in both the compressive and flexural strengths. After curing for 28 days, the compressive strength and flexural strength of the concrete sample prepared by grinding steel slag for 20 min increased by 7.45 MPa and 3.8 MPa compared with after curing for 3 days [27].

3.3. Impact of Mechanical Grinding on Phase Composition

Figure 5 shows the phase composition of the steel slag after different grinding times and the phase diagram of the steel slag concrete products. Specifically, Figure 5a shows the steel slag powder, Figure 5b shows the concrete with steel slag ground for 20 min, and Figure 5c shows the concrete with steel slag ground for 50 min.

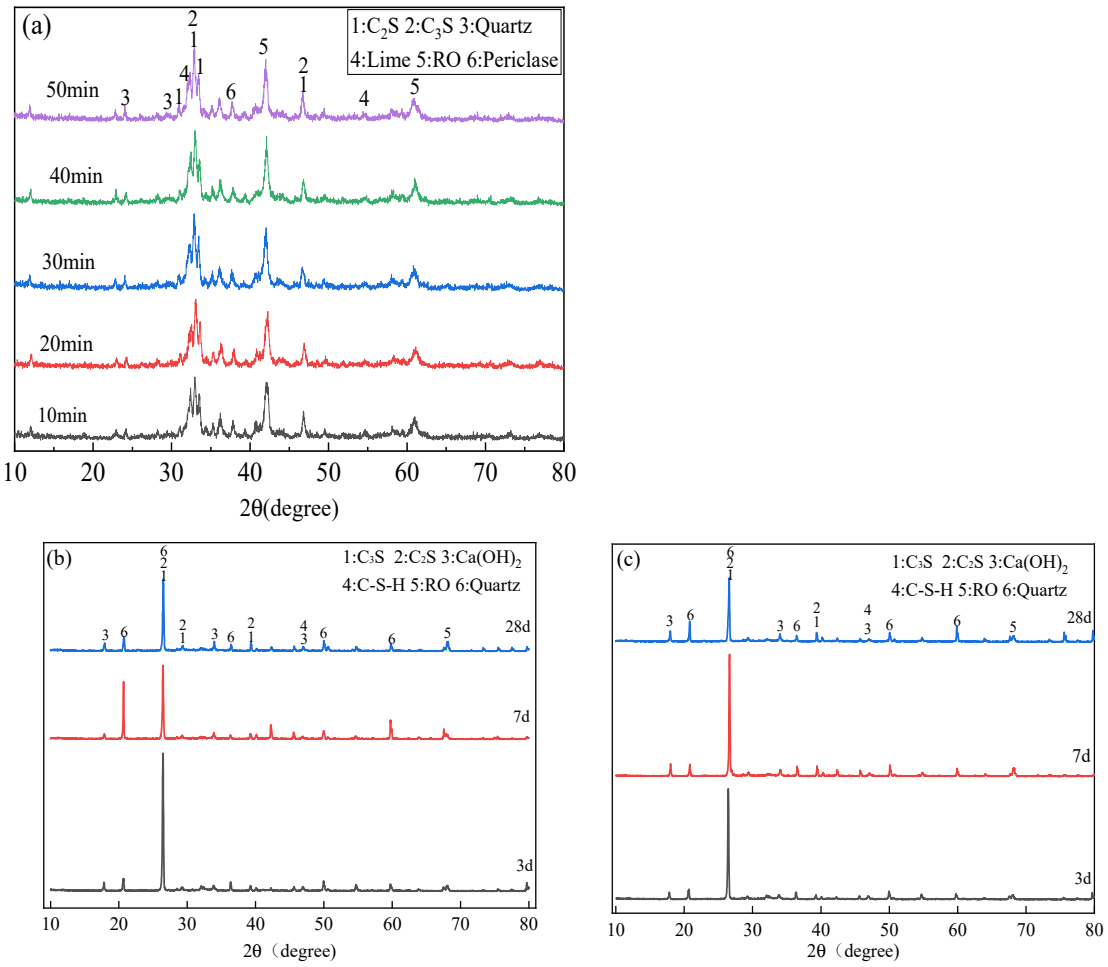


Figure 5. XRD pattern of the steel slag powder and steel slag concrete: (**a**) steel slag powder with different grinding time; (**b**) concrete with steel slag ground for 20 min; and (**c**) concrete with steel slag ground for 50 min.

In Figure 5a, it is evident that the mineral content of the steel slag is quite complex, mainly consisting of lime, periclase, C_2S, C_3S, quartz, and RO phases. Lime and periclase readily react with water to form $Ca(OH)_2$ and $Mg(OH)_2$, which is one of the reasons for the

poor stability of steel slag. After grinding for various durations, there are minor changes in the phase composition of the steel slag. At the 2θ = 24.04° and 2θ = 46.58° positions, the diffraction peaks of SiO_2, C_2S, and C_3S show a tendency to weaken and broaden. This is because the particles of the steel slag become finer with mechanical grinding and the crystals develop defects and distortions due to the applied forces. Consequently, the breaking of Si–O, Al–O, and other chemical bonds occurs at the lattice defects and distortions, forming amorphous reactive substances. This increases the content of the amorphous components and enhances the cementitious activity of the steel slag material [28].

In Figure 5b, it is evident that when the steel slag is ground for 20 min to prepare concrete, the main hydration products include C_2S, C_3S, $Ca(OH)_2$, RO phase, and C–S–H gel. The main phase composition of the hydration products of steel slag concrete is basically consistent with reference [29]. As the curing period increases, the diffraction peaks of C_2S, C_3S, and SiO_2 gradually weaken, indicating that the hydration reaction of the steel slag powder is ongoing. The clinker minerals C_2S, C_2F, and C_3S contained in the steel slag are not highly reactive, and C_2S and C_2F, as the main components of mineral clinker, produce a small amount of $Ca(OH)_2$ after the hydration reaction. The large amount of $Ca(OH)_2$ produced in the specimen is mainly generated by the CaO and f-CaO contained in the steel slag after the hydration reaction. The diffraction peak corresponding to $Mg(OH)_2$ is difficult to find, which is analyzed because the content of MgO contained in the steel slag is small, resulting in a small content of $Mg(OH)_2$ produced by the hydration reaction, and it may also be because some MgO is solidly dissolved in the RO phase (oxidized solid solution).

After grinding steel slag for 20 min, the D50 is reduced to 16.57 μm, indicating a significant increase in finer particles and a further reduction in the average particle size, thereby enhancing the reactivity. Consequently, the rate of the hydration reaction increases and reactive substances such as CaO and SiO_2 participate in the reaction system. At a 3-day age, hydration products like $Ca(OH)_2$ and C-S-H gel are formed. As the age increases to 7 and 28 days, the diffraction peak of $Ca(OH)_2$ gradually weakens, suggesting that $Ca(OH)_2$ is absorbed to produce other hydration products. The rapid formation of these hydration products not only improves the mechanical properties of the concrete but also mitigates the stability issues caused by CaO in the steel slag [30].

Figure 5c shows that when the steel slag is ground for 50 min to prepare concrete, the types of hydration products do not change compared to concrete prepared with steel slag ground for 20 min. Under the same curing age conditions, the diffraction peak intensities of $Ca(OH)_2$ and C–S–H are lower. This is because, after grinding the steel slag for 50 min, the D50 increases to 31.55 μm, indicating that the steel slag particles have become coarser. This coarsening of the particles affects the cementitious activity of the steel slag, resulting in fewer hydration products and weaker mechanical properties at the macroscopic level [31].

3.4. Influence of the Particle Size on the Microstructure

Figures 6–8 show the microstructural morphology of the steel slag concrete at different curing ages. Specifically, image (a) shows the concrete with no addition of steel slag, image (b) shows the concrete with steel slag ground for 20 min, and image (c) shows the concrete with steel slag ground for 50 min.

In Figure 6a, it is evident that in the concrete without steel slag, a large amount of fibrous and flocculent C–S–H gel has already formed at the 3-day age. These gels interlock and overlap with each other, establishing a solid framework within the microstructure, indicating a high degree of hydration. The early strength of the pure cement concrete sample is relatively high. Figure 6b,c show that the steel slag micro-powder has a retarding effect on the cement. After the steel slag powder particles encounter water, the Ca^{2+} and Mg^{2+} on the surface can dissolve, which rapidly increases the pH value of the liquid phase, promotes the formation of C–S–H gel and AFt, promotes the continuous hydrolysis of steel slag particles, increases the particle dissociation degree and the dissociated powder particles can absorb a certain amount of $Ca(OH)_2$ to form C–S–H gel. With the addition of steel slag, the degree of hydration is weaker, and only partial fibrous and flocculent C–S–H

gel is formed in the sample. However, the internal pores are larger, and the framework of the cementitious system is not yet fully interconnected [32].

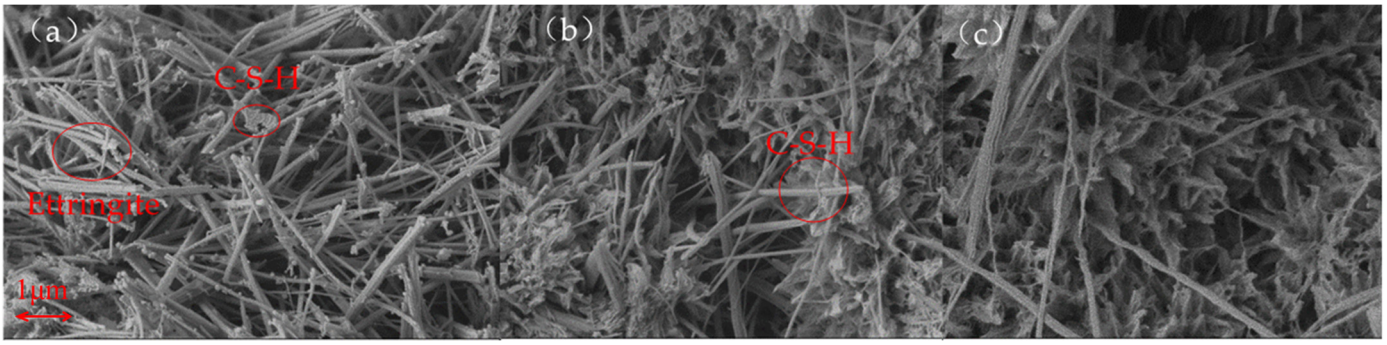


Figure 6. SEM image of the 3-day cured concrete product: (**a**) without steel slag; (**b**) steel slag ground for 20 min; and (**c**) steel slag ground for 50 min.

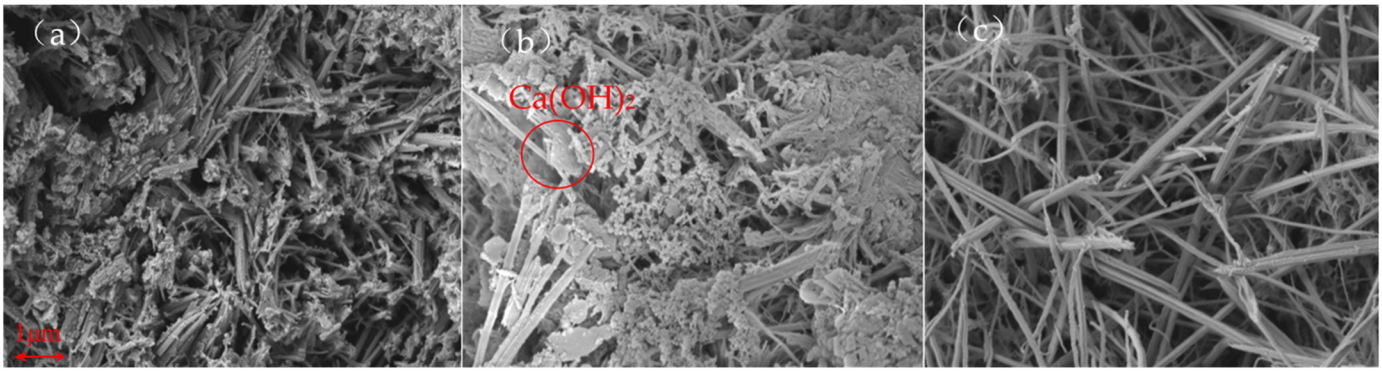


Figure 7. SEM image of the 7-day cured concrete product: (**a**) without steel slag; (**b**) steel slag ground for 20 min; and (**c**) steel slag ground for 50 min.

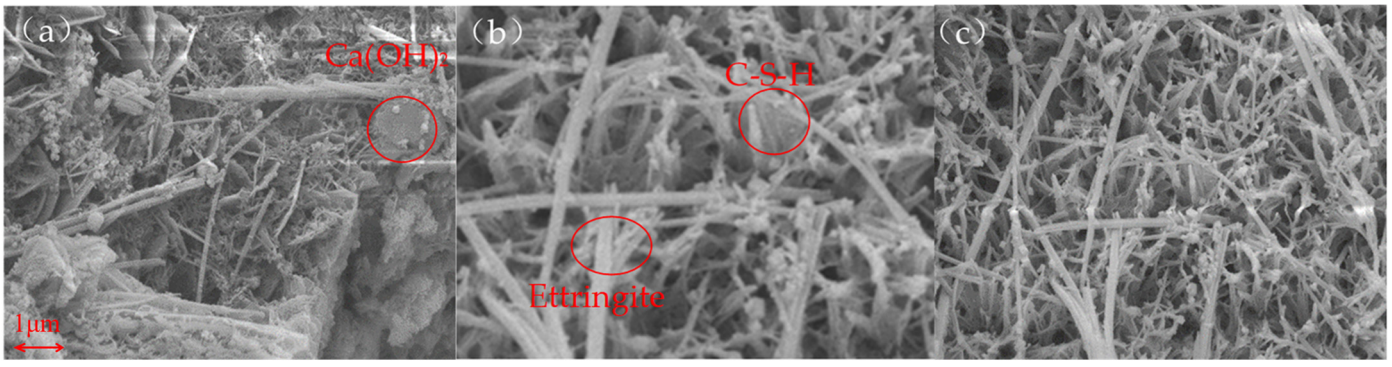


Figure 8. SEM image of the 28-day cured concrete product: (**a**) without steel slag; (**b**) steel slag ground for 20 min; and (**c**) steel slag ground for 50 min.

In Figure 7, compared to the 3-day age, the degree of hydration at 7 days is significantly higher. The hydration products become coarser and the mesh structure denser, resulting in higher compressive and flexural strengths at 7 days. At the same age, the sample with the steel slag ground for 50 min exhibits a slower hydration rate, with smaller and more delicate hydration product structures and more voids, which are noticeably lower than both the concrete with zero addition of steel slag and the concrete with steel slag ground for 20 min.

As illustrated in Figure 8, for the samples cured up to 28 days, the degree of hydration is further enhanced, resulting in the formation of abundant fibrous C–S–H gel and acicular

ettringite crystals [33]. These crystals are intricately interwoven and distributed, with fewer pores, forming a denser mesh structure, thereby further improving the mechanical properties. Since the average particle size of the steel slag ground for 20 min is smaller than that ground for 50 min, and with more small particles and greater specific surface area, the reactivity during hydration is more active. As a result, the number of ettringite crystals in the steel slag concrete is significantly higher than that in the steel slag concrete ground for 50 min. These crystals are coarser in size and more compact in structure, resulting in superior strength [34].

4. Conclusions

Based on the research conducted in this paper, the following conclusions are drawn:

(1) Mechanical grinding significantly affects the particle size and specific surface area of steel slag. As the grinding time increases, the specific surface area initially increases and then decreases, while the particle size shows a decreasing trend.
(2) The distribution of steel slag particles becomes narrower and more concentrated, with the cumulative particle size curve gradually shifting to the left. The optimal grinding time is 20 min.
(3) The incorporation of steel slag into concrete reduces the mechanical properties of the concrete. However, as the grinding time increases and the content of fine steel slag particles rises, the cementitious activity increases and the trend of reduced mechanical properties is mitigated.
(4) When the grinding time is 20 min, the steel slag has the smallest average particle size and the largest specific surface area, with D50 and D90 being 16.57 μm and 0.65 m^2/g, respectively; the 28-day compressive strength and flexural strength of the concrete reach 25.95 MPa and 7.40 MPa, respectively.
(5) Changes in the particle size of steel slag do not alter the types of hydration products in the concrete, but smaller particle sizes result in more hydration products, which are coarser in size and form a denser network structure. This leads to improved properties such as compressive strength and flexural strength.

Author Contributions: Conceptualization, investigation, methodology, writing—original draft, funding acquisition, M.L.; Investigation, project administration, Y.L. (Youjun Lu); Formal analysis, software, investigation, Y.L. (Yajuan Liu); Writing—review and editing, T.Z.; Investigation, supervision, J.C.; Investigation, validation, W.W. All authors have read and agreed to the published version of the manuscript.

Funding: This research was funded by the financial support from the Key R&D Projects of Ningxia Hui Autonomous Region, China (No. 2022BDE02002) and Fundamental Research Funds of the Central Universities, North Minzu University, China (No. 2021KJCX06).

Institutional Review Board Statement: Not applicable.

Informed Consent Statement: Not applicable.

Data Availability Statement: Data are contained within the article.

Conflicts of Interest: Author Yajuan Liu and Jingjun Chu were employed by the Ningxia Saima Kejin Concrete Co., Ltd. Author Wei Wang was employed by the Ningxia Hui Autonomous Region Construction Engineering Quality and Safety General Station. The remaining authors declare that the research was conducted in the absence of any commercial or financial relationships that could be construed as a potential conflict of interest.

References

1. Zhuo, K.X.; Liu, G.T.; Lan, X.W.; Zheng, D.P.; Wu, S.Q.; Wu, P.Z.; Guo, Y.C.; Lin, J.X. Fracture Behavior of Steel Slag Powder-Cement-Based Concrete with Different Steel-Slag-Powder Replacement Ratios. *Materials* **2022**, *15*, 2243. [CrossRef]
2. Zhuang, S.Y.; Wang, Q.; Luo, T. Modification of ultrafine blast furnace slag with steel slag as a novel high-quality mineral admixture to prepare high-strength concrete. *J. Build. Eng.* **2023**, *71*, 106501. [CrossRef]

3. Ning, S.K.; Jiang, X.D.; Li, B.; Shan, L.; Li, H.B. Research on Mechanical and Shrinkage Characteristics of a Resource-Based Cement Solid-Waste Concrete. *Materials* **2024**, *17*, 177. [CrossRef]
4. Aziz, I.H.; Abdullah, M.M.A.B.; Salleh, M.A.A.M.; Ming, L.Y.; Li, L.Y.; Sandu, A.V.; Nemes, O.; Mahdi, S.N. Recent Developments in Steelmaking Industry and Potential Alkali Activated Based Steel Waste: A Comprehensive Review. *Materials* **2022**, *15*, 1948. [CrossRef]
5. Rosales, J.; Agrela, F.; Díaz-López, J.L.; Cabrera, M. Alkali-Activated Stainless Steel Slag as a Cementitious Material in the Manufacture of Self-Compacting Concrete. *Materials* **2021**, *14*, 3945. [CrossRef]
6. Pradeep, K.; Shalinee, S. Utilization of steel slag waste as construction material: A review. *Mater. Today Proc.* **2023**, *78 Pt 1*, 145–152.
7. Wang, C.G.; Liu, Y.W.; Wang, S.; Ma, B.H.; Bi, G.H. Mechanical Properties and Durability of Double-Doped Steel Slag Concrete. *Bull. Chin. Ceram. Soc.* **2023**, *42*, 2846–2855. (In Chinese)
8. Zhou, M.; Cheng, X.; Chen, X. Studies on the Volumetric Stability and Mechanical Properties of Cement Fly-Ash-Stabilized Steel Slag. *Materials* **2021**, *14*, 495. [CrossRef]
9. Zhang, S.F.; Niu, D.T.; Wang, Y.; Tian, W.Q.; Luo, D.M.; Zhang, L. Insight into mechanical properties and microstructure of concrete containing steel slag and ground-granulated blast-furnace slag. *J. Sustain. Cem.-Based Mater.* **2023**, *12*, 1169–1180. [CrossRef]
10. Li, M.H.; Lu, Y.J.; Yang, S.L.; Chu, J.J.; Liu, Y.J. Study on the Early Effect of Excitation Method on the Alkaline Steel Slag. *Sustainability* **2023**, *15*, 4714. [CrossRef]
11. Nan, X.L.; Yang, X.; Zhang, Y.; Tang, W.B.; Zhang, F.Q. Study on Synergistic Hydration Mechanism of Steel Slag and Granulated Blast Furnace Slag. *J. Build. Mater.* **2024**, *2*, 1–13. (In Chinese)
12. Liu, J.P.; Hu, Z.Y.; Liu, P.; Wang, C.Y.; Wang, Y.S.; Zhang, W.X.; Li, X.H.; Pang, S.Y. Properties of alkali-activated furnace slag/steel slag cementitious materials mixed with silica fume and soda residue. *J. Shenyang Univ. Technol.* **2023**, *45*, 594–600. (In Chinese)
13. Masilamani, A.; Ramalingam, M.; Kathirvel, P.; Murali, G.; Vatin, N.I. Mechanical, Physico-Chemical and Morphological Characterization of Energy Optimised Furnace (EOF) Steel Slag as Coarse Aggregate in Concrete. *Materials* **2022**, *15*, 3079. [CrossRef]
14. Lai, M.H.; Zou, J.J.; Yao, B.Y.; Ho, J.C.M.; Zhuang, X.; Wang, Q. Improving mechanical behavior and microstructure of concrete by using BOF steel slag aggregate. *Constr. Build. Mater.* **2021**, *277*, 122269. [CrossRef]
15. Lai, M.H.; Chen, Z.H.; Wang, Y.H.; Ho, J.C.M. Effect of fillers on the mechanical properties and durability of steel slag concrete. *Constr. Build. Mater.* **2022**, *335*, 127495. [CrossRef]
16. Gencel, O.; Karadag, O.; Oren, O.H.; Bilir, T. Steel slag and its applications in cement and concrete technology: A review. *Constr. Build. Mater.* **2021**, *283*, 122783. [CrossRef]
17. Hao, S.; Luo, G.; Lu, Y.; An, S.L.; Song, W. Effect of High Temperature Reconstruction and Modification on Phase Composition and Structure of Steel Slag. *Minerals* **2023**, *13*, 67. [CrossRef]
18. Vitor, A.N.; Prannoy, S.; Bezerra, A.C.S.; Carlos, T.; Paulo, H.R.B. Influence of Activation Parameters on the Mechanical and Microstructure Properties of an Alkali-Activated BOF Steel Slag. *Appl. Sci.* **2022**, *12*, 12437.
19. Gao, T.M.; Dai, T.; Lei, S.; Li, J. Benefits of using steel slag in cement clinker production for environmental conservation and economic revenue generation. *J. Clean. Prod.* **2021**, *282*, 124538. [CrossRef]
20. Liao, Y.S.; Jiang, G.X.; Wang, K.J.; Qunaynah, S.A.; Yuan, W.J. Effect of steel slag on the hydration and strength development of calcium sulfoaluminate cement. *Constr. Build. Mater.* **2020**, *265*, 120301. [CrossRef]
21. Costa, L.C.B.; Nogueira, M.A.; Andrade, H.D.; Carvalho, J.M.F.D.; Elói, F.P.D.F.; Brigolini, G.J.; Peixoto, R.A.F. Mechanical and durability performance of concretes produced with steel slag aggregate and mineral admixtures. *Constr. Build. Mater.* **2022**, *318*, 126152. [CrossRef]
22. Sun, Y.; Chen, M.; Chen, D.; Liu, S.T.; Wu, S.P. Laboratory Preparation and Performance Characterization of Steel Slag Ultrafine Powder Used in Cement-Based Materials. *Sustainability* **2022**, *14*, 14951. [CrossRef]
23. Cui, X.W.; Leng, X.Y.; Nan, N.; Liu, X.; Zhang, M.T. Mechanical Activation Effect on the Performance of Steel Slag Particle Size Distribution and Cementitious Properties. *Bull. Chin. Ceram. Soc.* **2018**, *37*, 3821–3826. (In Chinese)
24. Huo, J.T.; Jiang, B.; Su, Y.; Fu, J.J.; Ma, M.Y.; He, X.Y. Influence of mechanical activation on cementitious characteristics of basic oxygen steelmaking slag. *Concrete* **2022**, *3*, 101–104+108. (In Chinese)
25. Jiang, L.; Wu, T.; Ma, L.F.; Han, X.; Chen, Y.H.; Han, F.L.; Bao, Y.W. Research on Grindability of Modified BOF Slag. *Bull. Chin. Ceram. Soc.* **2018**, *37*, 4034–4039. (In Chinese)
26. Roslan, H.H.; Ismail, M.; Abdul, M.Z.; Ghoreishiamiri, S.; Muhammad, B. Performance of steel slag and steel sludge in concrete. *Constr. Build. Mater.* **2016**, *104*, 16–24. [CrossRef]
27. Zhu, H.J.; Ma, M.Y.; He, X.Y.; Zheng, Z.Q.; Su, Y.; Yang, J.; Zhao, H. Effect of wet-grinding steel slag on the properties of Portland cement: An activated method and rheology analysis. *Constr. Build. Mater.* **2021**, *286*, 122823. [CrossRef]
28. Song, Y.; Lin, N.; Ma, Y.W.; Yang, L.; Shen, X.M.; Zheng, C.H.; Shan, J. Influence of Composite Activator on the Properties of Steel Slag and Slag Based Cementing Materials. *J. Anhui Univ. Technol. (Nat. Sci.)* **2019**, *36*, 24–28. (In Chinese)
29. Sun, X.G.; Liu, J.; Zhao, Y.Q.; Zhao, J.H.; Li, Z.H.; Sun, Y.; Qiu, J.P.; Zheng, P.K. Mechanical activation of steel slag to prepare supplementary cementitious materials: A comparative research based on the particle size distribution, hydration, toxicity assessment and carbon dioxide emission. *J. Build. Eng.* **2022**, *60*, 105200. [CrossRef]

30. Wang, J.F.; Chang, L.; Wang, Y.; Liu, H.; Yue, D.Y.; Cui, S.P.; Lan, M.Z. Research Status of Improving Cementitious Activity and Volume Stability of Steel Slag. *Mater. Rep.* **2023**, *37*, 119–127. (In Chinese)
31. Liu, M.Y.; Fang, Z.; Wu, J.; Zhan, J.H.; Peng, X.B. Analysis on Mechanical Properties and Microstructure of Multi-solid Waste Synergistic Reinforced Concrete. *J. Wuhan Univ. Technol.* **2023**, *45*, 55–62. (In Chinese)
32. Huang, X.; Yan, F.; Guo, R.; He, H. Study on the Performance of Steel Slag and Its Asphalt Mixture with Oxalic Acid and Water Erosion. *Materials* **2022**, *15*, 6642. [CrossRef] [PubMed]
33. Liu, Z.Y.; Ni, W.; Li, Y.; Ba, H.J.; Li, N.; Ju, Y.J.; Zhao, B.; Jia, G.L.; Hu, W.T. The mechanism of hydration reaction of granulated blast furnace slag-steel slag-refining slag-desulfurization gypsum-based clinker-free cementitious materials. *J. Build. Eng.* **2021**, *44*, 103289. [CrossRef]
34. Ji, Y.; Zhu, Y.C.; Zhu, G.; Liu, C.; Pu, F.F.; Liu, B.X. Preparation and Performance of Highly Active Steel Slag Powder. *J. Mater. Sci. Eng.* **2023**, *41*, 126–131+153. (In Chinese)

Disclaimer/Publisher's Note: The statements, opinions and data contained in all publications are solely those of the individual author(s) and contributor(s) and not of MDPI and/or the editor(s). MDPI and/or the editor(s) disclaim responsibility for any injury to people or property resulting from any ideas, methods, instructions or products referred to in the content.